Structure Properties Relationship of Donor–Acceptor Derivatives of Triphenylamine and 1,8-Naphthalimide

ARTICLE · JULY 2012

DOI: 10.1021/jp303172b

THE JOURNAL OF PHYSICAL CHEMISTRY C

Article

pubs.acs.org/JPCC

Structure Properties Relationship of Donor–Acceptor Derivatives of Triphenylamine and 1,8-Naphthalimide

Dalius Gudeika,[†] Asta Michaleviciute,[†] Juozas V. Grazulevicius,*[,†] Ramunas Lygaitis,[†] Saulius Grigalevicius,[†] Vygintas Jankauskas,[‡] Arunas Miasojedovas,[§] Saulius Jursenas,[§] and Gjergji Sini*[,⊥]

[†]Department of Organic Technology, Kaunas University of Technology, Radvilenu pl. 19, LT-50254 Kaunas, Lithuania

[‡]Department of Solid State Electronics, and [§]Institute of Applied Research, Vilnius University, Sauletekio 9, LT-10222 Vilnius, Lithuania

[⊥]Laboratoire de Physicochimie des Polymères et des Interfaces, EA 2528 Université de Cergy-Pontoise, 5 mail Gay-Lussac, 95031 Cergy-Pontoise Cedex, France

S *Supporting Information*

ABSTRACT: Solution-processable donor–acceptor molecules consisting of triphenylamine core and 1,8-naphthalimide arms were designed and synthesized by palladium-catalyzed Heck reaction. Dilute solutions of the synthesized compounds show strong absorption peaks in the visible wavelength range from 400 to 550 nm, which can be ascribed to the intramolecular charge transfer. Fluorescence quantum yields of dilute solutions of the synthesized materials range from 0.45 to 0.70, while those of the solid samples are in the range of 0.09–0.18. The synthesized molecules exhibit high thermal stability with the thermal degradation onset temperatures ranging from 431 to 448 °C. The compounds form glasses with glass-transition temperatures of 55–107 °C. DFT calculations show that HOMO and LUMO orbitals are almost entirely localized on the donor and acceptor moieties, respectively. Consequently, the frontier orbital energies for the three synthesized compounds are similar and practically do not depend on the number of 1,8-naphthalimide moieties. Ionization potentials of the solid samples (5.75–5.80 eV) are comparable. The charge-transporting properties of the synthesized materials were studied using xerographic time-of-flight method. Hole mobilities in the layers of the compounds having one and two 1,8-naphthalimide moieties exceed 10^{-3} $cm^2 \cdot V^{-1} \cdot s^{-1}$ at high electric fields at room temperature. The differences on the hole mobilities between the three synthesized compounds are discussed in the frame of Marcus theory by comparing the reorganization energy and electronic coupling parameters.

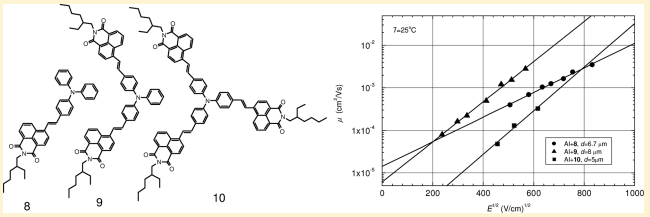

INTRODUCTION

Organic electroactive molecules having both donor and acceptor moieties are of increasing importance for the application in optoelectronic devices such as organic light-emitting diodes[1−3] and dye-sensitized[4,5] and bulk heterojunction[6] solar cells.

Organic molecules containing triphenylamine (TPA) units are of significant importance among the solution-processable amorphous organic molecular materials and have been intensively investigated for the applications in optoelectronic devices.[7] The TPA unit is in 3D propeller structure, which benefits the amorphous structure and solution processability of the molecules containing it. Moreover, TPA derivatives have good optical properties and hole-transporting ability.[1] On the other hand, 1,8-naphthalimide derivatives represent an attractive class of electron-deficient organic materials with high electron affinities.[8] They have wide energy gaps[9] and low reduction potentials.[10] The derivatives of TPA and 1,8-naphthalimide have been reported as sensitizers for dye-sensitized solar cells.[11]

In this work we report on the structure properties relationship of new donor–acceptor organic molecules with TPA fragment as core and 1,8-naphthalimide fragments as arms which were synthesized by palladium-catalyzed Heck reaction (see Scheme 1). It is expected that the absorption of these molecules will be extended to longer wavelengths due to intramolecular charge transfer between the donor and the acceptor units. The double bond linkage between TPA and 1,8-naphthalimide fragments will enhance the extent of conjugation degree which is also expected to result in the shift of absorption to longer wavelength region.

Joint experimental and theoretical approaches are employed in order to characterize the synthesized compounds and to better understand the structure–property relationships. In order to get some more insight in the hole-transport properties of these amorphous compounds, Marcus theory is applied by means of a comparative analysis of some molecular parameters

Received: April 3, 2012
Revised: June 26, 2012
Published: June 27, 2012

Scheme 1. Synthetic Route to 8−10

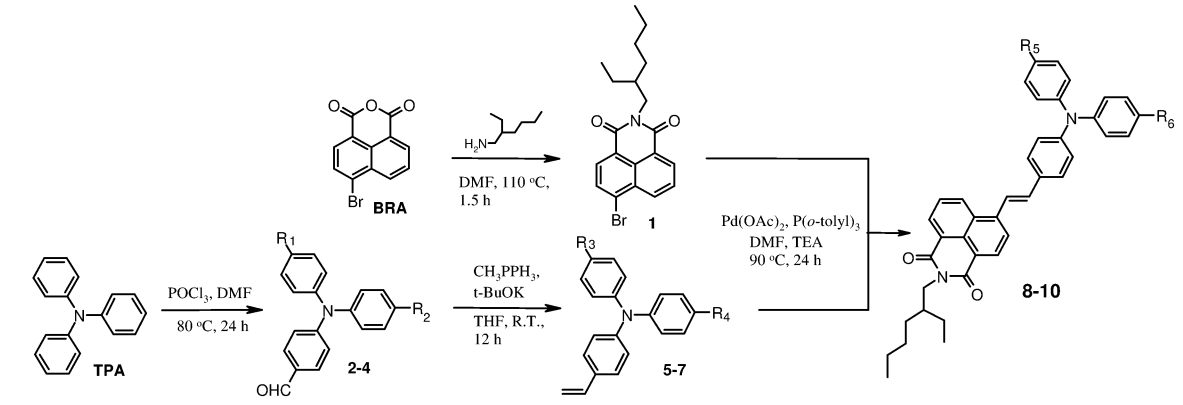

	R_1	R_2		R_3	R_4		R_5	R_6
2	H	H	**5**	H	H	**8**	H	H
3	H	CHO	**6**	H	$CH{=}CH_2$	**9**	H	CH=CH-**IM**
4	CHO	CHO	**7**	$CH{=}CH_2$	$CH{=}CH_2$	**10**	CH=CH-**IM**	CH=CH-**IM**

involved in the calculation of charge-transfer rate constants (k_{HT}).[12−15]

EXPERIMENTAL METHODS

Nuclear magnetic resonance (^{1}H NMR and ^{13}C NMR) spectra were obtained using a Varrian Unity Inova (300 MHz (^{1}H), 75.4 MHz (^{13}C)). All the data are given as chemical shifts in δ (ppm), multiplicity, integration downfield from $(CH_3)_4Si$. Mass (MS) spectra were obtained on a Waters ZQ 2000 (Milford, U.S.). Elemental analysis was performed with an Exeter Analytical CE-440 Elemental Analyzer. Infrared (IR) spectra were recorded using a Perkin-Elmer Spectrum GX spectrometer. UV spectra were recorded with a Hitachi U-3000 spectrometer. Fluorescence (FL) of the sample solutions and thin films was excited by 365 nm wavelength light-emitting diode (Nichia NSHU590-B) and measured using back-thinned CCD spectrometer (Hamamatsu PMA-11). Dilute solutions of the investigated compounds were prepared by dissolving them in spectral grade tetrahydrofuran (THF) at 10^{-6} M concentration. Neat films of the investigated compounds were casted from THF solutions on quartz substrates by drop-casting technique. Fluorescence quantum yield (QY) of the samples was estimated by using integrating sphere (Sphere Optics) coupled to the CCD spectrometer.[16] Melting points (mp) of the materials were measured on an Electrothermal MEL-TEMP melting point apparatus. Differential scanning calorimetry (DSC) measurements were carried out using a Perkin-Elmer DSC-7 series thermal analyzer at a heating rate of 10 °C/min under nitrogen flow. Thermogravimetric analysis (TGA) was performed on a METTLER TOLEDO TGA/SDTA 851^e. The solutions of the synthesized compounds with the concentration of 10^{-5} M were used for cyclic voltamperometry (CV) measurements. The electrochemical cell consisted of a three-electrode system, i.e., platinum rod as a counter electrode, glassy carbon as a working electrode, and $Ag/AgNO_3$ as the reference electrode. The measurements were carried out using 0.1 M tetrabutylammonium hexafluorophosphate ($TBAHFP_6$, Sigma Aldrich 99%) as electrolyte at room temperature in anhydrous dichloromethane (scan rate 50 $mV{\cdot}s^{-1}$). Charge mobilities (μ_h) were measured by xerographic time-of-flight method.[17,18] Ionization potentials (I_p) were established by electron photoemission technique in air.[19] The samples were prepared by the earlier reported procedure.[20] They were obtained by casting THF solutions of the materials on aluminum foil coated with the adhesive layer of methylmetacrylate and metacrylic acid copolymer. The samples before measurements were dried at 80 °C in air for 1 h.

Materials. 4-Bromo-1,8-naphthalic anhydride, 2-ethylhexylamine (TCI), triphenylamine (Aldrich), palladium acetate(II) (Aldrich), and tri-*o*-tolylphosphine (Fluka) were used as received. *N*,*N*-Dimethylformamide (DMF) was dried by distillation over CaH_2. Triethylamine was purified by distillation over KOH. All other reagents and solvents were commercially purchased and were used as supplied. Dichloromethane (POCH), ethyl acetate (Penta), *n*-hexane (Penta), and methanol (Penta) were purified and dried using the standard procedures.[21]

4-Bromo-*N*-(2-ethylhexyl)-1,8-naphthalimide (1). 1 was synthesized as described in the literature.[22] A solution of 4-bromo-1,8-naphthalic anhydride (1 equiv) in dimethylformamide (DMF) was added to a three-neck round-bottom flask equipped with a reflux condenser and a magnetic stirrer. Then 2-ethylhexylamine (1 equiv) was added dropwise, and the reaction mixture was heated up to 110 °C and stirred under nitrogen for 1.5 h. The end of the reaction was detected by TLC (eluent: toluene/diethyl ether, 6:1). The reaction mixture was concentrated using rotary evaporator, and then the product was precipitated into 1 N HCl, filtered off, and washed with 1 N HCl. The crude product was purified by silica gel column chromatography using acetone and hexane mixture (vol. ratio 1:1.5) as an eluent. After recystallization from the eluent mixture of solvents, yellow crystals were obtained. ^{1}H NMR spectrum (300 MHz, $CDCl_3$, δ, ppm): 8.70 (dd, 1H), 8.61 (dd, 1H), 8.45 (d, 1H), 8.08 (d, 1H), 7.89 (tr, 1H), 4.18−4.11 (m, 1H), 1.60−1.34 (m, 10H), 0.99−0.90 (m, 6H); mp = 82−83 °C.

4-(Diphenylamino)benzaldehyde (2). Phosphorus oxychloride (1.26 equiv) was added dropwise to DMF (1.47 equiv) at 0 °C, and the mixture was stirred for 1 h at this temperature. Then triphenylamine (1 equiv) was added, and the reaction mixture was stirred at 100 °C for 6 h. When the reaction was finished the mixture was cooled to room temperature, poured

dx.doi.org/10.1021/jp303172b | J. Phys. Chem. C 2012, 116, 14811−14819

into ice water, and neutralized to pH 7 with 5% NaOH aqueous solution. The solution was extracted with dichloromethane (3 × 150 mL). Then the organic phase was washed with water (2 × 100 mL) and dried over anhydrous $MgSO_4$. After filtration the solvent was removed. The crude product was purified by column chromatography using the eluent mixture of *n*-hexane and dichloromethane (vol. ratio 3:1). After recrystallization from the eluent mixture of solvents, white cystals were obtained. ^{1}H NMR spectrum (300 MHz, $CDCl_3$, δ, ppm): 10.19 (s, 1H), 7.95−7.69 (m, 2H), 7.58−6.57 (m, 12H); mp = 120−121 °C (lit.[23] 120−121 °C).

4,4′-Diformyl Triphenylamine (3). **3** was prepared by the same procedure as compound **2** using phosphorus oxychloride (1 equiv), DMF (1 equiv), and triphenylamine (0.4 equiv). The crude product was purified by silica gel column chromatography using the mixture of *n*-hexane and dichloromethane (vol. ratio 3:1) as an eluent. After recrystallization from the eluent mixture of solvents, the yellowish cystals were obtained. ^{1}H NMR spectrum (300 MHz, $CDCl_3$, δ, ppm): 9.87 (s, 2H), 7.79−7.13 (m, 13H); mp =143−144 °C (lit.[24] 142−145 °C).

Tris-(4-formylphenyl)amine (4).[25] **4** was prepared by the same procedure as compound **2** using phosphorus oxychloride (1 equiv), DMF (10 equiv) , and **3** (0.2 equiv). The crude product was purified by silica gel column chromatography using the eluent mixture of *n*-hexane and dichloromethane (vol. ratio 3:1). After recrystallization from the eluent mixture of solvents, the yellowish cystals were obtained. ^{1}H NMR spectrum (300 MHz, $CDCl_3$, δ, ppm): 9.92 (s, 3H), 7.83 (d, 6H), 7.25 (d, 6H); mp = 245−247 °C.

4-Vinyltriphenylamine (5). A mixture of **2** (1 equiv), sodium *tert*-butoxide (1.5 equiv), and CH_3PPh_3Br (1.2 equiv) in dry THF under nitrogen was heated with stirring at 80 °C for 24 h. After cooling to room temperature, the mixture was poured into distilled water and extracted with chloroform. The organic layer was dried with anhydrous magnesium sulfate and concentrated by vacuum evaporation. The crude product was purified by column chromatography (*n*-hexane/ethyl acetate vol. ratio 10:1) and then recrystallized from ethanol/acetone to obtain white crystals of **5**. ^{1}H NMR spectrum (300 MHz, $CDCl_3$, δ, ppm): 5.15 (d, 1H), 5.68 (d, 1H), 6.67 (dd, 1H), 6.92 (d, 2H), 7.00 (d, 4H), 7.04 (t, 2H), 7.30 (dd, 4H), 7.37 (d, 2H); mp = 90 − 91 °C (lit.[26] 91−92 °C).

4,4′-Divinyltriphenylamine (6). **6** was prepared by the same procedure as compound **5** using **3** (1 equiv), sodium *tert*-butoxide (3 equiv), and CH_3PPh_3Br (2.4 equiv). The crude product was purified by column chromatography (*n*-hexane/ethyl acetate vol. ratio 10:1). After recrystallization from the eluent mixture of solvents, white crystals of **6** were obtained. ^{1}H NMR spectrum (300 MHz, $CDCl_3$, δ, ppm): 7.24 (d, 4H), 7.19 (t, 2H), 7.09 (d, 2H), 6.97 (m, 5H), 6.68 (dd, 2H), 5.62 (d, 2H), 5.11 (d, 2H); mp = 62−63 °C (lit.[27] 64.5 °C).

Tris-(4-vinylphenyl)amine (7).[28] **7** was prepared by the same procedure as compound **5** using **4** (1 equiv), sodium *tert*-butoxide (4.5 equiv), and CH_3PPh_3Br (3.6 equiv). The crude product was purified by column chromatography (*n*-hexane/ethyl acetate vol. ratio 10:1). After recrystallization from the eluent mixture of solvents, white crystals of **7** were obtained. ^{1}H NMR spectrum (300 MHz, $CDCl_3$, δ, ppm): 7.24 (d, 6H), 6.62 (q, 6H), 5.67 (d, 3H) 5.16 (d, 3H); mp = 77−78 °C.

4-((*E*)-2-(*N*-(2-Ethylhexyl)-1,8-naphthalimid-4-yl)-vinyl)phenyl)benzenamine (8). A flask was charged with a mixture of **1** (0.50 g, 1.29 mmol), **5** (0.42 g, 1.55 mmol), $Pd(OAc)_2$ (5 mg, 0.016 mmol), P(*o*-tolyl)$_3$ (16 mg, 0.071 mmol), DMF (10 mL), and triethylamine (3 mL). The flask was degassed and purged with N_2. The mixture was heated at 90 °C for 24 h under N_2. Then, it was filtered, and the filtrate was poured into methanol. The orange precipitate was filtered and washed with methanol. The crude product was purified by dissolving it in THF and precipitating into methanol (0.35 g, 47%). It was recrystallized from methanol. Mp = 156−157 °C. ^{1}H NMR spectrum (300 MHz, $CDCl_3$, δ, ppm): 8.67 (dd, 1H, J_1 = 1.11 Hz, J_2 = 7.30 Hz, 5-$H_{Naphthalene}$), 8.64−8.61 (m, 2H, 7-$H_{Naphthalene}$, 3-$H_{Naphthalene}$), 8.03 (d, 1H, J = 7.97 Hz, 2-$H_{Naphthalene}$), 7.85−7.78 (m, 2H, 2-$H_{Naphthalene}$, =CH—), 7.56−7.53 (m, 2H, −Ar), 7.38−7.29 (m, 7H, −Ar, —CH=CH), 7.21−7.11 (m, 6H, −Ar), 4.18−4.11 (m, 2H, N−CH_2), 2.02−1.97 (m, 1H, −CH), 1.49−1.29 (m, 8H, −CH_2), 1.00−0.88 (m, 6H, −CH_3). IR (in KBr), cm^{-1}: 3033 ν(CH_{ar}); 2956, 2924, 2855 ν($CH_{aliphatic}$); 1695 ν(C=$O_{anhydride}$); 1655, 1584, 1508, 1491 ν(C=C_{ar}); 1354, 1231 ν(C−N); 965 γ(*trans*, —CH=CH); 778, 751, 695 γ(CH_{ar}). ^{13}C NMR spectrum (75.4 MHz, $CDCl_3$, δ, ppm): 143.43, 142.66, 140.76, 136.14, 132.75, 130.90, 130.48, 130.44, 129.31, 128.35, 128.31, 127.42, 126.93, 125.53, 125.35, 124.56, 122.83, 122.34, 122.29, 112.85, 54.74, 45.72, 38.62, 36.44, 33.13, 28.07, 27.89, 23.57, 15.31, 10.97. MS (APCI$^+$, 20 V), *m*/*z*: 578 ([M + H]$^+$). Anal. Calcd. for $C_{40}H_{38}N_2O_2$: C, 83.01; H, 6.62; N, 4.84. Found: C, 82.90; H, 6.67; N, 4.92.

4-((*E*)-2-(*N*-(2-Ethylhexyl)-1,8-naphthalimid-4-yl)-vinyl)-*N*-(4-((*E*)-2-(*N*-(2-ethylhexyl)-1,8-naphthalimid-4-yl)vinyl)phenyl)benzenamine (9). A flask was charged with a mixture of **1** (1.08 g, 2.78 mmol), **6** (0.30 g, 1.01 mmol), $Pd(OAc)_2$ (3.1 mg, 0.010 mmol), P(*o*-tolyl)$_3$ (9.2 mg, 0.041 mmol), DMF (20 mL), and triethylamine (6 mL). The flask was degassed and purged with N_2. The reaction mixture was heated at 90 °C for 24 h under N_2. Then, it was filtered, and the filtrate was poured into methanol. The red precipitate was filtered and washed with methanol and then dissolved in methylene chloride. After evaporation of the solvent, the crude product was purified by silica gel column chromatography using the mixture of ethyl acetate and *n*-hexane (vol. ratio 1:4) as an eluent and by recrystallization from methanol to obtain 0.60 g of red crystals of **6** with a yield of 65%. Mp = 179−180 °C. ^{1}H NMR spectrum (300 MHz, $CDCl_3$, δ, ppm): 8.69 (dd, 2H, J_1 = 1.02 Hz, J_2 = 7.29 Hz, 5,5′-$H_{Naphthalene}$), 8.64−8.61 (m, 4H, 7,7′-$H_{Naphthalene}$, 3,3′-$H_{Naphthalene}$), 8.03 (d, 2H, J = 7.79 Hz, 2,2′-$H_{Naphthalene}$), 7.88−7.79 (m, 4H, 6,6′-$H_{Naphthalene}$, =CH—), 7.60 (d, 4H, J = 8.60 Hz, −Ar), 7.41−7.33 (m, 5H, −Ar, =CH—), 7.26−7.19 (m, 6H, −Ar), 4.19−4.15 (m, 4H, N−CH_2), 2.08−1.92 (m, 2H, −CH), 1.52−1.25 (m, 16H, −CH_2), 1.02−0.86 (m, 12H, −CH_3). IR (in KBr), cm^{-1}: 3032 ν(CH_{ar}); 2956, 2924, 2855 ν($CH_{aliphatic}$); 1695 ν(C=$O_{anhydride}$); 1657, 1583, 1506, 1490 ν(C=C_{ar}); 1355, 1231 ν(C−N); 961 γ(*trans*, —CH=CH); 781, 753, 696 γ(CH_{ar}). ^{13}C NMR spectrum (75.4 MHz, $CDCl_3$, δ, ppm): 165.01, 164.66, 148.14, 147.05, 141.80, 134.88, 131.45, 130.21, 129.83, 129.73, 129.04, 128.43, 126.87, 125.73, 124.06, 123.88, 123.38, 123.39, 122.15, 121.44, 44.37, 38.20, 31.03, 29.00, 24.29, 23.37, 14.41, 10.95. MS (APCI$^+$, 20 V), *m*/*z*: 911 ([M + H]$^+$). Anal. Calcd. for $C_{62}H_{61}N_3O_4$: C, 81.64; H, 6.74; N, 4.61; O, 7.02. Found: C, 81.51; H, 6.80; N, 4.68.

4-((*E*)-2-(*N*-(2-Ethylhexyl)-1,8-naphthalimid-4-yl)-vinyl)-*N*-(4-((*E*)-2-(*N*-(2-ethylhexyl)-1,8-naphthalimid-4-yl)vinyl)-*N*-(4-((*E*)-2-(*N*-(2-ethylhexyl)-1,8-naphthalimid-4-yl)vinyl)phenyl)benzenamine (10). A flask was charged with a mixture of **1** (1.27 g, 3.27 mmol), **7** (0.25 g, 0.77 mmol),

dx.doi.org/10.1021/jp303172b | J. Phys. Chem. C 2012, 116, 14811−14819

$Pd(OAc)_2$ (2.6 mg, 0.084 mmol), $P(o\text{-tolyl})_3$ (7 mg, 0.031 mmol), DMF (30 mL), and triethylamine (9 mL). The flask was degassed and purged with N_2. The reaction mixture was heated at 90 °C for 24 h under N_2. Then, it was filtered, and the filtrate was poured into methanol. The red precipitate was filtered and washed with methanol and dissolved in methylene chloride. After evaporation of the solvent, the crude product was purified by silica gel column chromatography using the mixture of ethyl acetate and *n*-hexane (vol. ratio 1:8) as an eluent and by recrystallization from methanol to obtain 0.42 g of red crystals of **6** with a yield of 44%. Mp = 209−210 °C. ^{1}H NMR spectrum (300 MHz, $CDCl_3$, δ, ppm): 8.67 (dd, 3H, J_1 = 0.96 Hz, J_2 = 7.25 Hz, 5,5′,5″-$H_{Naphthalene}$), 8.64−8.61 (m, 3H, 7,7′,7″-$H_{Naphthalene}$, 3,3′,3″-$H_{Naphthalene}$), 8.04 (d, 3H, J = 7.89 Hz, 2,2′,2″-$H_{Naphthalene}$), 7.91−7.79 (m, 6H, 6,6′,6″-$H_{Naphthalene}$, −vinylic), 7.65 (m, 6H, −Ar), 7.41−7.27 (m, 9H, −Ar, ═CH—), 4.18−4.16 (m, 6H, N−CH_2), 2.07−1.95 (m, 3H, −CH), 1.47−1.31 (m, 24H, −CH_2), 1.00−0.91 (m, 18H, −CH_3). IR (in KBr), cm^{-1}: 3032 $\nu(CH_{ar})$; 2954, 2925, 2856 $\nu(CH_{aliphatic})$; 1698 $\nu(C{=}O_{anhydride})$; 1656, 1583, 1504, 1461 $\nu(C{=}C_{ar})$; 1354, 1231 ν(C−N); 956 γ(*trans*, —CH═CH); 778, 753, 724 $\gamma(CH_{ar})$. ^{13}C NMR spectrum (75.4 MHz, $CDCl_3$, δ, ppm)): 164.92, 164.76, 147.67, 141.62, 134.73, 132.29, 131.54, 131.54, 131.43, 130.09, 129.75, 129.04, 128.64, 126.97, 124.78, 123.96, 123.43, 122.64, 122.46, 121.49, 44.43, 38.21, 30.97, 29.00, 24.33, 23.38, 14.42, 10.96. MS (APCI$^+$, 20 V), *m*/*z*: 1244 ($[M + H]^+$). Anal. Calcd. for $C_{84}H_{84}N_4O_6$: C, 81.00; H, 6.80; N, 4.50. Found: C, 79.75; H, 6.85; N, 4.48.

Computational Details. The computations were carried out by mean of density functional methods (DFT)[29] employing the B3LYP[30] functional, in conjunction with the 6-31G(d,p) basis set. The geometry optimizations of the model compounds M-**8**, M-**9**, and M-**10** (containing methyl substituents instead of the experimental alkyl ones) were performed in the absence of medium effects. In the case of M-**10** model compound, a *C*3 symmetry was imposed. However, the symmetry-relaxed optimizations result in similar structures. Different isomers around the double ethylenic moieties were considered, and the lowest one was considered for subsequent calculations. All the geometry optimizations were followed by frequency calculations to ensure that real minima were obtained. The geometry optimizations of the cationic radical species were performed at the unrestricted open-shell level.

Time-dependent density functional theory method (TDDFT)[31] was used for the study of the spectroscopic properties of the molecules. Up to 40 excited states were calculated, and the theoretical absorption bands were obtained by considering a band half-width of 0.2 eV at half-height (Gaussview 5 software).

The vertical ionization potentials (I_p) were calculated at the B3LYP/6-31G(d,p) level as energy difference between neutral and radical cation species at the neutral state geometry. In order to check for any methodology influence on these values, other functionals (M052X,[32] BMK,[33] wB97X-D,[34] wB97X[35]) and different basis sets (6-31G(d,p), 6-311+G(2d,p)) were considered.

The internal reorganization energy (λ_i) values of model compounds **8**−**10** were calculated at the B3LYP/6-31G(d,p) level according to the following equation:[36]

$$\lambda_i = \lambda_i^1 + \lambda_i^2 = (E_M^{geom(M^+)} - E_M^{geom(M)}) + (E_{M^+}^{geom(M)} - E_{M^+}^{geom(M^+)})$$

In this equation the quantity $E_M^{geom(M^+)}$, for instance, corresponds to the energy of the neutral molecule (M) in the geometry of the cationic species (M^+).

All the computations were performed with Gaussian 09 program.[37]

RESULTS AND DISCUSSION

Synthesis and Characterization. The synthetic route to donor−acceptor glass-forming derivatives (**8**−**10**) is shown in Scheme 1.

The first step was condensation of 4-bromo-1,8-naphthalic anhydride with 2-ethylhexylamine in DMF to obtain 4-bromo-*N*-(2-ethylhexyl)-1,8-naphthalimide (**1**). Aldehydes (**2**−**4**) were obtained under the conditions of the Vilsmeier reaction. Compounds **5**−**7** were prepared by the reaction of aldehydes (**2**−**4**) with methyltriphenylphosphonium bromide. The final step was Heck reactions of bromide **1** with 4-vinyltriphenylamine (**5**), 4,4'-divinylphenylamine (**6**), and tris-(4-vinylphenyl)amine (**7**) in the presence of palladium(II) acetate and tri-*o*-tolylphosphine to obtain the target compounds **8**−**10**.

The chemical structures of the synthesized compounds were confirmed by ^{1}H NMR, ^{13}C NMR, FT-IR, mass spectrometries, and elemental analysis. Compounds **8**−**10** were readily soluble in common organic solvents like dichloromethane, chloroform, THF, acetonitrile, and toluene.

Geometries and Frontier Orbitals. The geometries of M-**8**, M-**9**, and M-**10** model compounds (containing methyl groups instead of longer-chain alkyl groups) are presented in Figure 1.

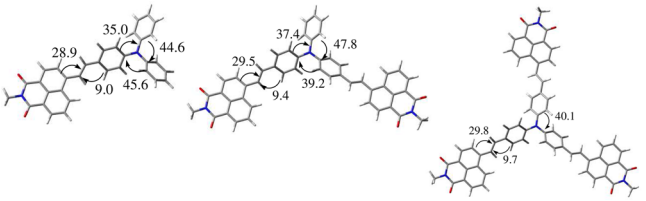

Figure 1. Optimized geometries of M-**8** (left), M-**9** (center), and M-**10** (right) model compounds, obtained at the B3LYP/6-31G(d,p) level. Some relevant dihedral angles (absolute values in degrees) are shown.

Some relevant geometrical parameters are also indicated. In the three molecules the geometry around the central N atom is planar ("N-plane"), due to the π-conjugation between the phenyl groups and the lone pair of the central N atom. The dihedral angles of each phenyl group with the "N-plane" are approximately 44−47° for the unsubstituted phenyl rings and 35−40° for the substituted ones (angles increasing with the number of 1,8-naphthalimide fragments in the arms). The frontier orbitals for the three molecules are given in Figure 2.

The three HOMO orbitals are very similar, being localized almost entirely on the TPA core, containing only small antibonding contributions from the ethylene moieties. Similar HOMO energies should be then expected for these compounds suggesting similar electronic and optical properties.

Thermal Properties. The thermal behavior of compounds **8**−**10** was studied by TGA materials. The temperatures of the onsets of their thermal degradation are in the range of 431−448 °C (Table 1). The thermal stability of the synthesized donor−acceptor derivatives increases with increase of the number of 1,8-naphthalimide arms. The temperatures of the onsets of

dx.doi.org/10.1021/jp303172b | J. Phys. Chem. C 2012, 116, 14811−14819

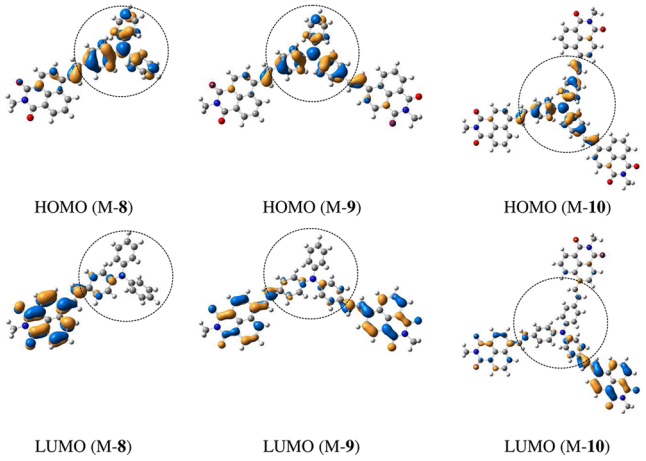

Figure 2. Pictograms of frontier orbitals for the model compounds M-**8**, M-**9**, and M-**10**. The encircled parts delimit the TPA moiety.

Table 1. Thermal Characteristics of Compounds 8−10

molecule	T_g (°C)[a] (2nd heating)	T_m (°C)[a]	T_{ID} (°C)
8	55	163	431
9	90	185	445
10	107	222	448

[a]Determined by DSC, scan rate 10 °C/min, N_2 atmosphere. T_m, temperature at melting; T_g, glass-transition temperature; T_{ID}, thermal decomposition onset.

thermal degradation of compounds **8**−**10** are higher than those of the earlier reported carbazolyl-substituted derivatives of triphenylamine.[38]

Compounds **8**−**10** were isolated after the synthesis as crystalline materials. Their behavior in DSC experiments was similar; therefore, DSC curves of only one compound are given in Figure 3.

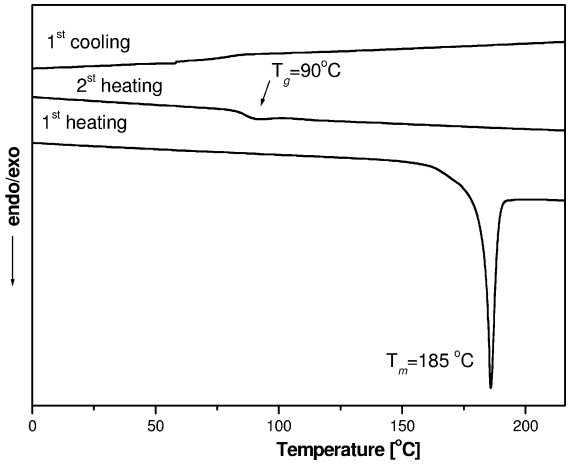

Figure 3. DSC thermograms of compound **9** (scan rate of 10 °C/min, N_2 atmosphere).

Temperatures of thermal transitions of compounds **8**−**10** are summarized in Table 1. The first run heating scans revealed only melting endotherms. No crystallization was observed during the cooling scans. In the second heating scans compounds **8**, **9**, and **10** showed glass transitions at 55, 90, and 107 °C, respectively and no crystallization was observed in the following heating and cooling scans. The glass-transition temperatures (T_g) of compounds **9** and **10** are high enough for their possible application in optoelectronic devices such as organic light-emitting diodes. The values of both T_g and melting points increase with the increase of the number of 1,8-naphthalimide arms. This observation can apparently be explained by the increase of molecular size and enhancement of intermolecular interaction. T_g of compound **10** is by ca. 30 °C higher than that of carbazolyl-trisubstituted triphenylamine with the same alkyl group at the nitrogen atom.[38]

Optical Properties. Absorption and FL spectra of dilute solutions in THF of compounds **8**−**10** are shown in Figure 4.

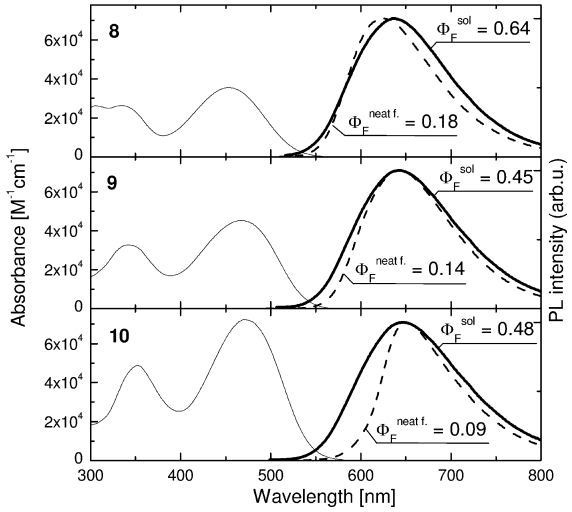

Figure 4. UV−vis and FL (λ_{ex} = 365 nm) spectra of dilute THF solutions and of neat films of **8**−**10** compounds.

The wavelengths of the absorption and fluorescence maxima and fluorescence quantum yields are summarized in Table 2.

Table 2. Optical and Photophysical Characteristics of 8−10

	solution λ_{max} (nm)		film λ_{max} (nm)			
compd	UV	FL	UV	FL	Stokes shift (nm) sol/film	Φ_F sol/film
8	455	641	470	624	186/154	0.64/0.18
9	469	643	489	643	174/154	0.45/0.14
10	474	646	490	652	172/162	0.48/0.09

The absorption edges of compounds **8**−**10** are considerably red-shifted with respect of those of carbazolyl- and fluorenyl-substituted derivatives of triphenylamine.[37] They are also red-shifted with respect to the absorption edges of the derivatives of triphenylamine and 1,8-naphthalimide in which the two moieties are linked via imide linkage.[39]

The lowest energy absorption bands of these compounds which can be ascribed to the charge transfer exhibit bathochromic and hyperchromic shifts with the increase of the number of 1,8- naphthalimide arms. All compounds show a broad structureless long-wavelength absorbance band with strongly Stokes-shifted broad fluorescence typical for intra-moleculer charge-transfer states. The solutions of all the compounds (**8**−**10**) also show absorption bands peaking at ca. 350 nm. These absorption bands can be assigned to $\pi-\pi^*$ transition of naphthalimide groups.[40] The dilute solutions of these compounds emit orange light peaking in the range of

dx.doi.org/10.1021/jp303172b | J. Phys. Chem. C 2012, 116, 14811−14819

641−646 nm when excited with the ultraviolet irradiation. Incorporation of additional 1,8-naphthalimide arms weakly affects the emissive states. The spectra of the solid samples of compounds **8**−**10** exhibit small red shifts with respect to those of the dilute solutions, probably due to the smaller dihedral angles in the solid state, thus giving rise to more efficient π-conjugation end decreased HOMO−LUMO gap. The TDDFT calculations also support the charge-transfer nature of the lowest energy band. The theoretical UV−vis spectra for the model compounds M**8**−M**10** are shown in Figure S1 (Supporting Information). The $S_0 \rightarrow S_1$ excitation in compound **8** is entirely due to HOMO → LUMO electronic transition, with HOMO and LUMO orbitals being almost entirely localized on the donor and acceptor moieties, respectively (Figure 2). In the case of compound **9**, a second CT excitation ($S_0 \rightarrow S_2$) of smaller oscillator strength (0.163 as compared to 1.044 for $S_0 \rightarrow S_1$) is present in the CT band (Figure S1, Supporting Information). The $S_0 \rightarrow S_2$ excitation corresponds to HOMO → LUMO+1 electronic transition. It is worth pointing out here that LUMO and LUMO+1 orbitals of compound **9** (containing two 1,8-naphthalimide arms) are the in-phase and out-of-phase combinations of the local LUMO orbitals of each 1,8-naphthalimide arm. Similar observations can be done in the case of compound **10**, with the difference that the two CT electronic transitions (HOMO → LUMO, LUMO +1) are degenerate, hence corresponding to identical oscillator strengths (0.876). The roughly linearly increasing intensity of the charge-transfer bands from **8** to **10** is thus related to the presence (in the compounds **9** and **10**) of a second CT transition ($S_0 \rightarrow S_2$) of increasing intensity in the same order.

The other bands seem to contain some mixing of CT and local excitations. The important Stokes shifts observed for all compounds (Table 2) can also be traced back to the large geometrical reorganizations happening after HOMO → LUMO(LUMO+1) transitions, which is suggested by the totally different space localization of the HOMO and LUMO orbitals for each compounds. Theoretical calculations are complemented by measurements of absorption and FL spectra of **8**−**10** compounds in dilute solutions of different polarity solvents (Figure S4, Supporting Information). The lowest energy absorption band is bathochromically shifted by 13, 18, and 24 nm for compounds **8**−**10**, respectively, with the increase of dielectric constant of the solvent. The intensity of the lowest energy absorption band decreases with the increase of the solvent polarity and the number of 1,8- naphthalimide arms. More pronounced bathochromic spectral shift was observed for FL spectra of investigated naphthalimide derivatives. The maximum intensity wavelengths of fluorescence spectra shifted with the change of the solvent from toluene to DMSO to longer wavelengths for ca. 182, 184, and 208 nm for compounds **8**−**10**, respectively.

The fluorescence quantum yields of the dilute solutions in THF of **8**−**10** range from 0.64 to 0.45, while those of the films are considerably lower and range from 0.09 to 0.18. The highest fluorescence quantum yields both for solution and for the solid sample were observed for compound **8**. The fluorescence quantum yields of dilute solutions strongly depend on the solvent polarity (Figure S4, Supporting Information). The largest FL QY of 0.70 was observed for compounds **9** and **10** with larger number of 1,8- naphthalimide arms in nonpolar solvent toluene. The compounds show significant decrease of the FL QY down to 0.01 in polar solvent dimethylsulfoxide.

Electrochemical Properties. We used CV for the investigation of the redox behavior of compounds **8**−**10** and for the estimation of their highest occupied molecular orbital (HOMO) and lowest unoccupied molecular orbital (LUMO) energy levels. The CV curves of **8**−**10** are shown in Figure 5. Table 3 summarizes the relevant data.

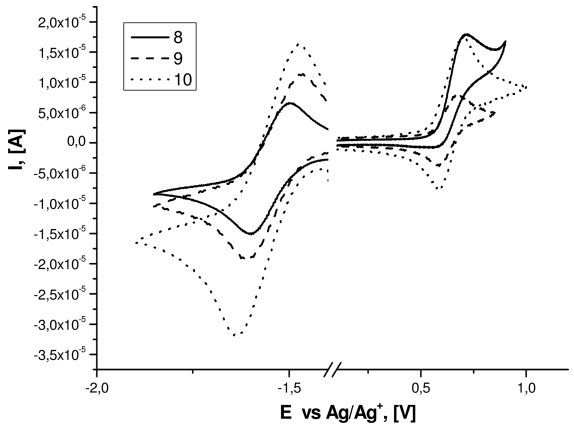

Figure 5. Cyclic voltammograms of **8**−**10** (10^{-5} M solutions, scan rate of 50 mV s^{-1} vs Ag/Ag^+) in 0.1 M solution of $TBAHFP_6$ CH_2Cl_2.

All the compounds (**8**−**10**) were found to be electrochemically stable. Their cyclic voltammograms show one quasi-reversible oxidation and reduction couple waves. The shapes of CV curves are similar for all compounds. The oxidation part of the CV curves is principally related to the oxidation of the triphenylamino group, and the reduction part is related to the reduction of imido group, which is also suggested from the shape of the HOMO and LUMO orbitals (see pictograms in Figure 2).

On the basis of the onset potentials, we estimated HOMO levels of **8**, **9**, and **10** to be −5.18, −5.24, and −5.25 eV, respectively, with LUMO energy levels of −3.06, −3.07, and −3.08 eV, respectively, according to the energy level of the ferrocene reference (−4.8 eV).[41] The small range of the HOMO energies (0.07 eV) is due to their similar shape for the three compounds (almost total localization of this orbital on the TPA core, Figure 2). The slight decrease of the HOMO energies from **8**−**10** is related to the electron-withdrawing nature of 1,8-naphthalimide arms. Similar arguments can explain the small range and the trend of the LUMO energies.

The band-gap value is one of the most useful characteristics for materials used in optoelectronic devices. The electrochemically estimated band gaps (E_g^{elc}) of **8**−**10** were 2.12−2.17 eV, and they were slightly lower than the corresponding optical band gap (E_g^{opt}) 2.27−2.34 eV (Table 3), but within the range of error (0.2−0.5 eV).[42]

Photoelectrical Properties. Amorphous thin films on substrates could be prepared by casting or spin-coating techniques from the materials reported in this work. Figure 6 shows a electron photoemission spectra of the layers of compounds **8**−**10** recorded in air.

The values of ionization potentials obtained by extrapolation of the straight parts of the spectra to the *X*-axis are given in Table 3. The values of ionization potentials (I_p) of the films of compounds **8**−**10** range from 5.75 to 5.80 eV. These values are very similar and comparable to those of triphenylamine (TPA) derivatives.[43,44] It seems that the introduction of 1,8-naphthalimide arms and the increase of the number of these

dx.doi.org/10.1021/jp303172b | J. Phys. Chem. C 2012, 116, 14811−14819

Table 3. HOMO−LUMO Energy Levels, Optical and Electrochemical Band-Gap Energies, and Ionization Potentials of 8−10

molecule	E_{HOMO} (eV)[a]	E_{LUMO} (eV)[b]	E_g^{elc} (eV)[c]	E_g^{opt} (eV)[d]	I_p (eV)[e]
8	−5.18 (−5.17)[f]	−3.06 (−2.45)[f]	2.12	2.34	5.75 (6.33)[f]
9	−5.24 (−5.29)[f]	−3.07 (−2.63)[f]	2.17	2.28	5.78 (6.28)[f]
10	−5.25 (−5.39)[f]	−3.08 (−2.72)[f]	2.17	2.27	5.80 (6.26)[f]

[a] $E_{HOMO} = -(E_p + 4.8)$ (eV). [b] $E_{LUMO} = -(E_n + 4.8)$ (eV) (where E_n and E_p are onset reduction and oxidation potentials versus the Fc/Fc^+). [c] Having HOMO and LUMO bands value, it is simple to calculate electrochemical band gap $E_g^{elc} = E_{LUMO} - E_{HOMO}$ (eV). [d] The optical band gap estimated from the onset wavelength of optical absorption according to the formula $E_g = 1240/\lambda_{edge}$, in which the λ_{edge} is the onset value of absorption spectrum in long-wave direction. [e] Established from electron photoemission in air spectra. [f] Corresponding to the model compounds M-**8**, M-**9**, and M-**10** calculated at the B3LYP/6-31G(d,p) level.

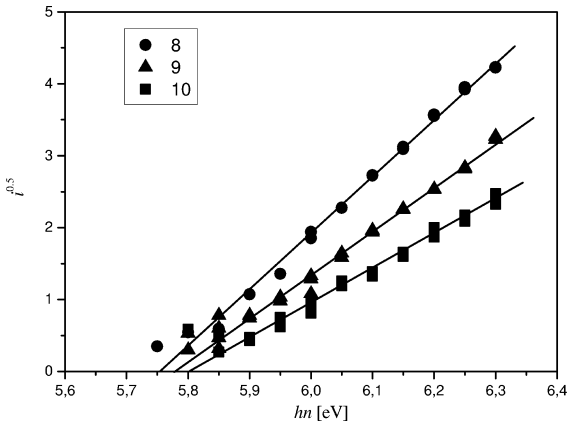

Figure 6. Electron photoemission spectra of the layers of **8−10**.

arms has a negligible effect on the ionization potentials of the TPA derivatives. In the frame of Koopmans' theorem (relating in this case the first I_p values to the HOMO energies), these observations can be explained by the similarity between the HOMO orbitals of compounds **8−10** on the one hand and the HOMO (TPA) on the other hand (Figure 2).

The slightly increasing experimental I_p values (from 5.75 to 5.80 eV) can be explained at first sight in a straightforward maner: on the basis of Koopmans' theorem, the decreasing HOMO energies from **8** to **10** (Table 3) can explain the increasing experimental I_p values in the same order. However, the theoretical results indicate that the picture is slightly different, while the theoretical HOMO (and LUMO) energies decrease from M**8** to M**10** (in line with the above explanation), the theoretical I_p values decrease (from 6.33 to 6.26 eV) instead of increasing. This result is intriguing as it is at odds with the trends deduced from the Koopmans' theorem and the experimental results. In order to check for possible bad performances in the applied theoretical methods, medium effects, different DFT methods, and different basis sets were considered (Computational Details). However, similar results were obtained in all cases. It is worth pointing out that the ranges of the experimental and theoretical I_p values are both very small (0.05 and 0.07 eV, respectively). The discrepancies reported so far might then be due to the influence of other factors such as (i) the fact that the orbital-relaxation energy terms between the neutral and cationic species are ignored in the Koopmans' theorem ("frozen orbital" approximation), which can be on the origin of the different I_p trends deduced from the Koopmans' theorem and from the direct calculations; (ii) the quite different T_g values between **8** and **9** or **10** (Table 1) indicate different molecular packing properties, which also might influence the trend of the I_p values. We conclude this point by underlying that the relevant result to retain here is the very small range of the I_p values obtained (experimentally and theoretically) for the three compounds **8−10**, which is principally due to the similar nature of their HOMO orbitals.

The time-of-flight technique was used to study charge-transport properties of the derivatives of triphenylamine and 1,8-naphthalimide. Figure 7 shows the electric field dependencies of the hole-drift mobilities of the amorphous layers of **8−10**.

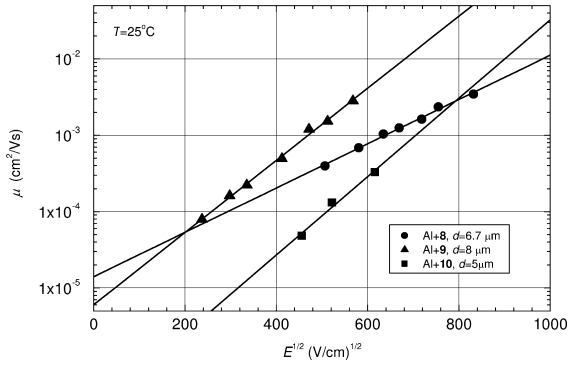

Figure 7. Electric field dependencies of hole-drift mobilities in charge-transport layers of neat films of compounds **8−10**.

The layers of compounds **8−10** demonstrated hole-drift mobility values in the range from 10^{-4} to 10^{-3} $cm^2 \cdot V^{-1} \cdot s^{-1}$ at moderate electric fields at room temperature. Hole mobilities in the layers of the compounds **8** and **9** having one and two 1,8-naphthalimide moieties well exceeded 10^{-3} $cm^2 \cdot V^{-1} \cdot s^{-1}$ at high electric fields. Dispersive hole transport was observed for the layers of compounds **8−10**. For the illustration of this statement representative TOF transients of holes for compound **8** are shown in Figure 8.

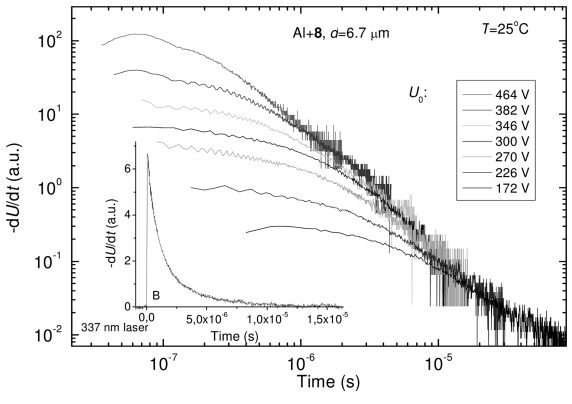

Figure 8. Representative TOF transients of the layer of compound **8**.

dx.doi.org/10.1021/jp303172b | J. Phys. Chem. C 2012, 116, 14811−14819

In every case, the short initial spike, limited by the time resolution of measurement setup, is followed first by a clear constant current plateau and then by a drop. In order to get some more insight in the hole-transport properties of these compounds, a qualitative discussion of charge-transfer rate constants (k_{HT}) based on the Marcus theory can be helpful.[45−48]

In the case of amorphous materials, the rate constant of a hole-transfer reaction between two adjacent molecules can be described by the "hopping" mechanism and calculated by means of the following equation:[11−14]

$$k_{HT} = \frac{4\pi^2}{h}\frac{1}{\sqrt{4\pi\lambda k_B T}}t^2 \exp\left[\frac{-(\Delta G^\circ + \lambda)^2}{4k_B T\lambda T}\right] \quad (1)$$

In this equation, t is the electronic coupling between two adjacent molecules, ΔG° is the free energy of the hole-transfer reaction (approximated to zero in the case of charge hopping between identical molecules in the absence of electric field), and λ is the reorganization energy. This last parameter is the sum of two terms: (i) λ_s, containing the contribution from the medium polarization energy, and (ii) λ_i, representing the energetic effort due to the intramolecular geometric relaxations related to the hole transfer between two adjacent molecules.

Equation 1 indicates that in order to obtain high hole-transfer rate constants (k_{HT}), the reorganization energy (λ) should be small whereas the electronic coupling parameter (t) should be large. In the following only these two molecular parameters will be discussed, whereas the influence of morphological and other structural parameters will be ignored.

In the frame of Marcus theory, the medium reorganization energy (λ_s) depends on the size of the species, which, in view of the similar HOMO distribution (Figure 2), can be assumed to remain practically constant across the three compounds. The internal reorganization energy (λ_i) values of model compounds **8**−**10** (0.18, 0.14, and 0.11 eV, respectively, B3LYP/6-31G(d,p) level) are small and vary in a narrow range. The relatively small λ_i values for the three compounds suggest good hole-transfer properties, which seems in line with the high hole mobilities measured for compounds **8** and **9**. On the other hand, the trend of λ_i values (**8** > **9** > **10**) suggests increasing hole-transfer rate constants (k_{HT}) in the order **8** < **9** < **10** which seems in disagreement with the experimental trend of the hole mobilities (**10** < **8** < **9**). This discrepancy, along with the narrow range of λ_i values (0.07 eV), indicates that from the microscopical viewpoint the hole transfer in these compounds should be dominated by the electronic coupling between the HOMO orbitals of adjacent molecules.

The electronic coupling parameter is strongly dependent on the overlap between the HOMO orbitals of adjacent molecules. The HOMO pictograms in Figure 2 suggest that in order for these compounds to exhibit good hole-transfer properties, a sufficient spatial overlap should be established between the TPA cores. In the case of compound **10**, the TPA core is hindered by three 1,8-naphthalimide arms, which prevent from efficient approach of the TPA cores of two adjacent molecules. In the case of **8** and **9**, there are still one or two phenyl rings nonsubstituted by 1,8-naphthalimide arms, thus suggesting less hindered overlap between adjacent HOMO orbitals. However, while this observation might give ideas on why compound **10** exhibits lower hole mobilities than **8** and **9**, the higher mobility of **9** as compared to **8** seems in to be disagreement with the above argument. Other factors should consequently dominate in the comparison of hole mobilities between **8** and **9**. We suspect that the different packing manners between **8** and **9**, as suggested by the very different T_g values (Table 1), indicate stronger intermolecular interactions in **9** as compared to compound **8**, which might result in smaller mean intermolecular distances, hence larger electronic coupling in compound **9**.

CONCLUSIONS

Three new donor−acceptor glass-forming derivatives with triphenylamine core and 1,8-naphthalimide arms were synthesized and characterized. Their thermal, optical, electrochemical, and photoelectrical properties were studied and discussed in terms of correlation with their chemical structures. The molecules showed high thermal stability with the thermal degradation onset temperatures ranging from 431 to 448 °C. The compounds form glasses with glass-transition temperatures being in the range of 55−107 °C. Electron photoemission spectra of the amorphous films of the materials revealed ionization potentials similar to those of the derivatives of triphenylamine (5.75−5.80 eV) with no evidence of dependence of ionization potentials on the number of 1,8-naphthalimide arms. This is traced back to the similar nature of the HOMO orbitals for the three compounds, which are localized almost entirely on the triphenylamino donor moiety. The compounds exhibit strong long-wavelength absorbance in the 455−474 nm range which is due to intramolecular charge-transfer transitions. The intensity of the charge-transfer bands enhances almost linearly with the number of incorporated 1,8-naphthalimide arms which is due to the increasing number and strength of the charge-transfer transitions in the same order. Compound **10** with three 1,8-naphthalimide arms exhibits the highest emission quantum yield of 0.70 in nonpolar toluene dilute solution. Charge-transporting properties of the synthesized materials were studied by xerographic time-of-flight technique. Dispersive hole transport was observed for all the synthesized compounds. Hole mobilities in the layers of the compounds having one and two 1,8-naphthalimide moieties well exceeded 10^{-3} $cm^2 \cdot V^{-1} \cdot s^{-1}$ at high electric fields at room temperature. The differences of the values of hole mobilities between these compounds are supposed to be related to the different hindering of the triphenylamino cores of these molecules by the 1,8-naphthalimide arms, which influences the HOMO overlap and electronic coupling between two adjacent molecules.

ASSOCIATED CONTENT

Supporting Information

UV−vis experimental and theoretical spectra of M-**10**, M-**9**, and M-**8** model compounds obtained by mean of TDDFT calculations at the B3LYP/6-31G(d,p) level; pictogram of the HOMO orbital for the neutral triphenylamine (TPA) compound and pictograms of some relevant orbitals for the neutral model compounds M**8**−M**10**; absorbance and fluorescence spectra of the solutions of compounds **8**−**10** in various solvents. This material is available free of charge via the Internet at http://pubs.acs.org.

AUTHOR INFORMATION

Corresponding Author

*E-mail: juozas.grazulevicius@ktu.lt (J.V.G.); gjergji.sini@u-cergy.fr (G.S.).

Notes

The authors declare no competing financial interest.

■ ACKNOWLEDGMENTS

This research was funded by a Grant No. MIP-063/2011 from the Research Council of Lithuania. A.M. acknowledges EU Structural Funds project "Postdoctoral Fellowship Implementation in Lithuania" for funding her postdoctoral fellowship. Habil. Dr. V. Gaidelis from the Department of Solid State Electronics, Vilnius University is thanked for the help in the measurements of ionization potentials.

■ REFERENCES

(1) Shirota, Y.; Kageyama, H. *Chem. Rev.* **2007**, *107*, 953−1010.
(2) Chaskar, A.; Chen, H. F.; Wong, K. T. *Adv. Mater.* **2011**, *23*, 3876−95.
(3) Duan, L.; Qiao, J.; Su, Y.; Qiu, Y. *Adv. Mater.* **2011**, *23*, 1137−1144.
(4) Hagfeldt, A.; Boschloo, G.; Sun, L.; Kloo, L.; Petterssson, H. *Chem. Rev.* **2010**, *110*, 6595−6663.
(5) Yum, J. H.; Hagberg, D. P.; Moon, S. J.; Karlsson, K. M.; Marinado, T.; Sun, L.; Hagfeldt, A.; Nazeeruddin, M. K.; Grätzel, M. *Angew. Chem., Int. Ed. Engl.* **2009**, *48*, 1576−1580.
(6) Boudreault, P. L. T.; Najari, A.; Leclerc, M. *Chem. Mater.* **2011**, *23*, 456−469.
(7) He, C.; He, Q.; Yi, Y.; Wu, G.; Bai, F.; L.; Shuai, Z.; Li, Y. *J. Mater. Chem.* **2008**, *18*, 4085−4090.
(8) Cacialli, F.; Friend, R. H.; Bouche, C. M.; Le Barny, P.; Facoetti, H.; Soyer, F.; Robin, P. *J. Appl. Phys.* **1998**, *83*, 2343−2356.
(9) Wintges, V.; Valat, P.; Kossanyi, J.; Demeter, A.; Biczok, L.; Berces, T. *New J. Chem.* **1996**, *20*, 1149−1158.
(10) Martin, E.; Weigand, R. *Chem. Phys. Lett.* **1998**, *288*, 52−58.
(11) Huang, X.; Fang, Y.; Li, X.; Xie, Y.; Zhu, W. *Dyes Pigm.* **2011**, *90*, 297−303.
(12) Marcus, R. A. *Rev Mod Phys.* **1993**, *65*, 599−610.
(13) Levich, V. G. *Adv. Electrochem. Electrochem. Eng.* **1966**, *4*, 249−371.
(14) Marcus, R. A. *J. Chem. Phys.* **1956**, *24*, 966−978.
(15) Marcus, R. A.; Sutin, N. *Biochim. Biophys. Acta* **1985**, *821*, 265−322.
(16) Mello, J. C.; Wittmann, H. F.; Friend, R. H. *Adv. Mater.* **1997**, *9*, 230−232.
(17) Montrimas, E.; Gaidelis, V.; Pazera, A. *Lithuanian J. Phys.* **1996**, *6*, 569−578.
(18) Vaezi-nejad, S. M. *Int. J. Electron.* **1987**, *62*, 361−384.
(19) Miyamoto, E.; Yamaguchi, Y.; Yokoyama, M. *Electrophotography.* **1989**, *28*, 364−370.
(20) Kirkus, M.; Tsai, M. H.; Grazulevicius, J. V.; Wu, C. C.; Chi, L. C.; Wong, K. T. *Synth. Met.* **2009**, *159*, 729−734.
(21) Harwood, L. M.; Moody, C. J. *Organic Chemistry. Principles and Practice*; Blackwell Science: Boston, MA, 1989.
(22) Gudeika, D.; Lygaitis, R.; Mimaitė, V.; Grazulevicius, J. V.; Jankauskas, V.; Lapkowski, M.; Data, P. *Dyes Pigm.* **2011**, *91*, 13−19.
(23) Wang, X. M.; Zhou, Y. F.; Yu, W. T.; Wang, C.; Fang, Q.; Jiang, M. H.; Lei, H.; Wang, H. Z. *J. Mater. Chem.* **2000**, *10*, 2698−2703.
(24) Seok, J. H.; Park, S. H.; El-Khouly, M. E.; Araki, Y.; Ito, O.; Key, K. J. *J. Organomet. Chem.* **2009**, *694*, 1818−1825.
(25) Wang, H. Y.; Chen, G.; Xu, X. P.; Ji, S. J. *Synth. Met.* **2010**, *160*, 1065−1072.
(26) Yeh, K. M.; Lee, C. C.; Chen, Y. *Synth. Met.* **2008**, *158*, 565−571.
(27) Behl, M.; Seekamp, J.; Zankovych, S.; Sotomayor Torres, C. M.; Zentel, R.; Ahopelto, J. *Adv. Mater.* **2002**, *8*, 588−591.
(28) Feng, J.; Zhang, C.; Li, Y.; Yang, M. J. *Appl. Polym. Sci.* **2011**, *121*, 217−225.
(29) Kohn, W.; Sham, L. *J. Phys. Rev.* **1965**, *140*, A1133−A1138.
(30) (a) Lee, C. T.; Yang, W. T.; Parr, R. G. *Phys. Rev. B* **1988**, *37*, 785−789. (b) Becke, A. D. *J. Chem. Phys.* **1993**, *98*, 5648−5652.
(31) (a) Gross, E .K. U.; Kohn, W. *Phys. Rev. Lett.* **1985**, *55*, 2850−2852. (b) Runge, E.; Gross, E. K. U. *Phys. Rev. Lett.* **1984**, *52*, 997−1000. (c) Gross, E. K. U.; Kohn, W. *Adv. Quantum Chem.* **1990**, *21*, 255−291. (d) Bauernschmitt, R.; Ahlrichs, R *Chem. Phys. Lett.* **1996**, *256*, 454−464. (e) Casida, M. E.; Jamorski, C.; Casida, K. C.; Salahub, D. R. *J. Chem. Phys.* **1998**, *108*, 4439−4449.
(32) Zhao, Y.; Schultz, N. E.; Truhlar, D. G. *J. Chem. Theory Comput.* **2006**, *2*, 364−382.
(33) Boese, A. D.; Martin, J. M. L. *J. Chem. Phys.* **2004**, *121*, 3405−3416.
(34) Chai, J. D.; Head-Gordon, M. *Phys. Chem. Chem. Phys.* **2008**, *10*, 6615−6620.
(35) Chai, J. D.; Head-Gordon, M. J. *Chem. Phys.* **2008**, *128*, 084106−084121.
(36) Bredas, J. L.; Beljonne, D.; Coropceanu, V.; Cornil, J. *Chem. Rev.* **2004**, *104*, 4971−4982.
(37) Frisch, M. J.; Trucks, G. W.; Schlegel, H. B.; Scuseria, G. E.; Robb, M. A.; Cheeseman, J. R.; Scalmani, G.; Barone, V.; Mennucci, B.; Petersson, G. A.; et al. *Gaussian 09*, revision B.01; Gaussian Inc.: Wallingford, CT, 2010.
(38) Sonntag, M.; Kreger, K.; Hanft, D.; Strohriegl, P.; Setayesh, S.; de Leeuw, D. *Chem. Mater.* **2005**, *17*, 3031−3039.
(39) Takahashi, S.; Nozaki, K.; Kozaki, M.; Suzuki, S.; Keyaki, K.; Ichimura, A.; Matsushita, T.; Okada, K. *J. Phys. Chem. A* **2008**, *112*, 1046−1055.
(40) McMasters, S.; Kelly, L. A. *J. Phys. Chem. B* **2006**, *110*, 2533−2542.
(41) Pommerehne, J.; Vestweber, H.; Guss, W.; Mahrt, R. F.; Bässler, H.; Porsch, M.; Daub, J. *Adv. Mater.* **1995**, *7*, 551−554.
(42) Chen, W. C.; Liu, C. L.; Yen, C. T.; Tasi, F. C.; Tonzola, C. J.; Olson, N.; Jenekhe, S. A. *Macromolecules* **2004**, *37*, 5959−5964.
(43) Keruckas, J.; Lygaitis, R.; Simokaitiene, J.; Grazulevicius, J. V.; Jankauskas, V.; Sini, G. *J. Mater. Chem.* **2012**, *22*, 3015−3027.
(44) Mimaite, V.; Ostrauskaite, J.; Gudeika, D.; Grazulevicius, J. V.; Jankauskas, V. *Synth. Met.* **2011**, *161*, 1575−1581.
(45) Marcus, R. A. *Rev. Mod. Phys.* **1993**, *65*, 599−610.
(46) Levich, V. G. *Adv. Electrochem. Electrochem. Eng.* **1966**, *4*, 249−371.
(47) Marcus, R. A. *J. Chem. Phys.* **1956**, *24*, 966−978.
(48) Marcus, R. A.; Sutin, N. *Biochim. Biophys. Acta* **1985**, *821*, 265−322.